Malyukin *et al. Nanoscale Research Letters* (2017) 12:566
DOI 10.1186/s11671-017-2339-7

Nanoscale Research Letters

NANO EXPRESS **Open Access**

Oscillations of Cerium Oxidation State Driven by Oxygen Diffusion in Colloidal Nanoceria (CeO_{2-x})

Yuri Malyukin[1*], Vladimir Klochkov[1], Pavel Maksimchuk[1], Vladyslav Seminko[1] and Nikolai Spivak[2]

Abstract

The redox performance of CeO_{2-x} nanocrystals (nanoceria) is always accompanied by the switching of cerium oxidation state between Ce^{3+} and Ce^{4+}. We monitored $Ce^{3+} \rightarrow Ce^{4+}$ oxidation of nanoceria stimulated by oxidant in aqueous colloidal solutions controlling the luminescence of Ce^{3+} ions located at different distances from nanoceria surface. The observed Ce^{3+} luminescence changes indicate that $Ce^{3+} \rightarrow Ce^{4+}$ reaction develops inside nanoceria being triggered by the diffusing oxygen originated from the water splitting on oxidized nanoceria surface. We present the first observation of the pronounced oscillations of Ce^{3+} luminescence intensity arising from $Ce^{3+} \leftrightarrow Ce^{4+}$ reversible switching. This threshold effect is to be driven by uptaking and releasing oxygen by nanoceria, when the concentration of oxygen vacancies in nanoceria lattice, oxidant concentration in colloidal solution, and temperature reach certain critical values. So, the ability of nanoceria to uptake and release oxygen depending on the environmental redox conditions really makes it the self-sufficient eternal antioxidant.

Keywords: Oxygen vacancies, Clusters, Luminescence, Antioxidants

Background

Today, nanocrystals with different structure and chemical composition are widely used in great diversity of modern applications [1–9]. Along with important engineering utilizations [3, 4], CeO_2 nanocrystals (nanoceria) gave birth to promising biomedical developments [5–9] owing to its ability to work as a regenerative scavenger of reactive oxygen species (ROS). The main prerequisite that makes nanoceria so unique and useful is generally attributed to high content of oxygen vacancies (V_O) and Ce^{3+} ions on its surface [10–14]. In nanoceria lattice, V_O and Ce^{3+} ions are interrelated defects [10–14]; two Ce^{3+} ions are accounted for one V_O [13]. The defect (Ce^{3+}, V_O) concentration in nanoceria can be controlled by particle size, special doping, and temperature treatment [11, 14, 15]. In general, the surface oxygen can assist the redox cycle through V_O creation and healing or surface V_O can act as binding sites for catalytically active species [3, 4, 14]. The surface Ce^{3+} ions of nanoceria are commonly supposed to provide ROS scavenging due to switching between 3+ and 4+ oxidation states [5–9]. ROS, namely superoxide ions O_2^-, hydroxyl radicals $OH^{\cdot}$, and hydrogen peroxide H_2O_2 at low concentrations, are critically important for the regulation of cell functions [5–9]. Unlike ordinary antioxidants, which disappear irretrievably after interaction with ROS [5–7], nanoceria, at particle sizes below 15 nm, can act as a self-regenerating antioxidant [5–9]. The critical dependence of nanoceria biological activity on its size, as well as the self-regeneration mechanism of nanoceria in biological environment, is still poorly understood [5–7], and discussions are continuing [8, 9]. It should be stressed that in in vitro and in vivo experiments [5–9], the nanoceria operate at a high defect concentration and water activity and its redox performance can be strongly masked by the cell antioxidant systems.

So, to understand the mechanism of nanoceria redox performance, we used more simple and controlled conditions: the nanoceria oxidation dynamics was studied in aqueous colloidal solutions for nanoceria specimens with variation of oxygen deficiency. As V_O (Ce^{3+}) concentration vary with the particle size [10–12], the nanoceria specimens of 3.0, 10.0, and 50.0 nm were used. According to

---

* Correspondence: malyukin@isma.kharkov.ua
[1] Institute for Scintillation Materials, National Academy of Sciences of Ukraine, 60 Nauky Ave, Kharkiv 61001, Ukraine
Full list of author information is available at the end of the article

the data [12], V_O concentration in 3.0-nm nanoceria can reach up to ~ 20%. We determined that V_O concentration in 10.0-nm nanoceria, as compared with 3.0-nm nanoceria, was twice less (see Additional file 1). In the case of 50.0-nm nanoceria, doping with Y^{3+} (or Eu^{3+}) ions and vacuum annealing were used to generate V_O and to create different conditions for oxygen diffusion in nanoceria lattice [14, 15]. In all 50.0 nm samples, V_O concentration was made equivalent to 10.0-nm nanoceria. At Re^{3+} doping of 50.0-nm nanoceria, the concentrations of Y^{3+} and Eu^{3+} ions were at the level of 10 at.% (see Additional file 1). These concentrations were sufficiently lower than the values of corresponding solubility limits for these ions in ceria lattice, ~ 25 at.% [16] or even ~ 45 at.% [17] for Y^{3+} ions and ~ 30 at.% [18] for Eu^{3+} ions; so, formation of Y_2O_3 or Eu_2O_3 phases can be excluded. All colloidal solutions contained the same amount of the substance (1.0 g/l) and were characterized by initial pH ~ 7. For nanoceria oxidation, hydrogen peroxide (HP) and potassium periodate KIO_4 (PP) were used. PP allowed us to exclude the chemical diversity of HP. The details of the nanoceria synthesis and characterization of the obtained specimens, as well as a description of the experiments, are presented in the Additional file 1.

Results and Discussion

Relying on our preliminary experiment [19], the Ce^{3+} luminescence (Fig. 1a) due to the dipole-allowed 5d → 4f optical transitions of Ce^{3+} ions [20] was used to monitor the oxidation dynamics of all tested nanoceria specimens. The increase of the Ce^{3+} band asymmetry with the decrease of particle size, that is, with the increase of the surface-to-bulk ratio (see insert in Fig. 1a) indicates clearly its inhomogeneity. The long-wave part of this band can be attributed to the Ce^{3+} luminescence from the nanoceria subsurface layer, and the remaining part of the Ce^{3+} band comes from deep-seated Ce^{3+} ions. The subsurface Ce^{3+} ions have the red-shifted luminescence spectra (see insert in Fig. 1a) because of the weakening of the crystal field acting on these ions as a result of the lattice parameter increase in the direction to the nanoceria surface [12]. Contrary to 3.0-nm nanoceria, for 50.0-nm nanoceria, the impact of these ions to the resulting luminescence spectrum is negligible (see insert in Fig. 1a). This attribution was confirmed by the stronger Forster quenching [21] of the long-wave part of the Ce^{3+} band (see Additional file 1 and Fig. 1b). The increase of the quencher concentration resulted in the luminescence quenching of deeper lying Ce^{3+} ions (Fig. 1b) because of the reduction of the donor-acceptor distance [21].

Adding oxidant (HP or PP) to colloidal solutions resulted in a decrease of the Ce^{3+} band intensity for all tested nanoceria specimens (Fig. 1a). Moreover, one can see that under selective quenching of the Ce^{3+} band (Fig. 1b), the oxidant stimulated a drop in luminescence of the deep-seated Ce^{3+} ions (see insert in Fig. 1b). The Ce^{3+} → Ce^{4+} oxidation occurs for these ions as well in spite of the fact that the oxidant cannot penetrate into nanoceria. This effect is similar to annealing nanoceria in oxygen atmosphere (see Additional file 1). Hence, the oxidant stimulates the penetration of oxygen (its source will be determined below) inside nanoceria. It is really corroborated by the defect-controlled time evolution

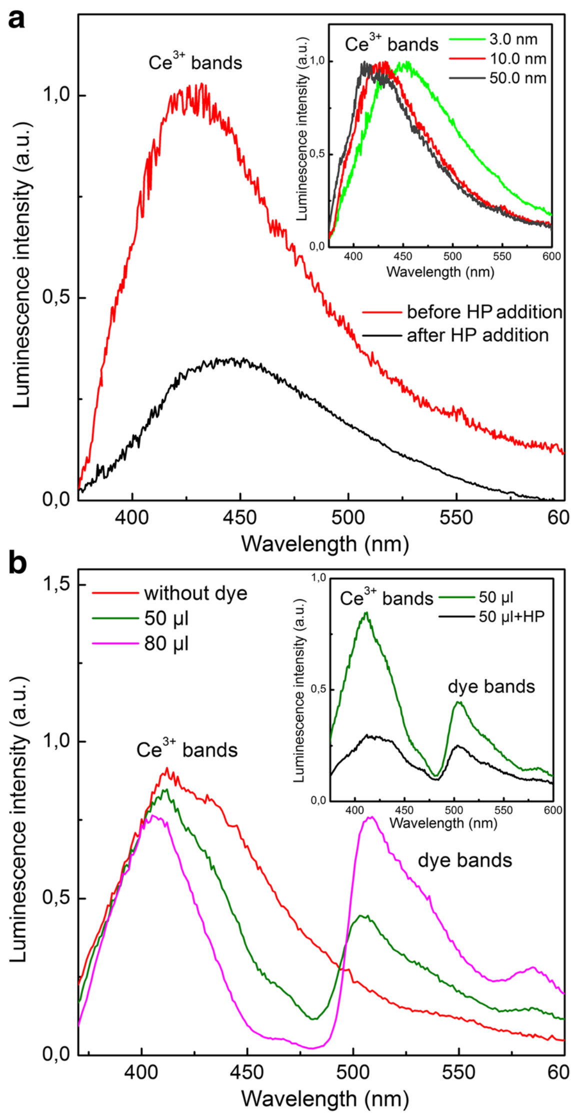

Fig. 1 Luminescence spectra of nanoceria under different conditions. **a** 10.0-nm nanoceria before and 25 min after HP ($C = 0.1$ mM) addition. Insert: normalized spectra of different nanoceria samples. **b** Luminescence spectra of 10.0-nm nanoceria before and after addition of 50 and 80 µl of dye. Insert: spectra of 10.0-nm nanoceria after addition of 50 µl of dye and subsequent addition of HP ($C = 0.1$ mM)

of Ce^{3+} luminescence under oxidant action (Fig. 2a). In this experiment, both HP and PP act in a similar way (see insert in Fig. 2a). As follows from Fig. 2a, the 3.0-nm nanoceria with the highest V_O concentration demonstrated the fastest drop of the Ce^{3+} band intensity and the lowest residual Ce^{3+} luminescence. At the same V_O concentration, the Y^{3+}-doped nanoceria showed a stronger quenching rate of the Ce^{3+} band intensity and lower level of residual Ce^{3+} luminescence as compared to the Eu^{3+}-doped nanoceria (Fig. 2a). It correlates with the fact that the activation energy of oxygen diffusion in cerium oxide increases in the presence of Eu^{3+} ions in a stronger way than of Y^{3+} ions [14, 15]. Hence, the Ce^{3+} band intensity decrease under oxidant action (Figs. 1 and 2a) is a result of $Ce^{3+} \rightarrow Ce^{4+}$ oxidation caused by oxygen penetration into nanoceria via the vacancy mechanism of diffusion [14, 15]. The addition of the reducing agent (for example, benzenetriol) to the colloidal solution upon nanoceria oxidation did not lead to the Ce^{3+} luminescence recovery, which is consistent with the proposed mechanism of $Ce^{3+} \rightarrow Ce^{4+}$ oxidation inside nanoceria.

The lower water concentration in the colloidal solution slowed down the dynamics of nanoceria oxidation (Fig. 2b), while the increase of initial pH accelerated this process (see insert in Fig. 2b). Excluding possible

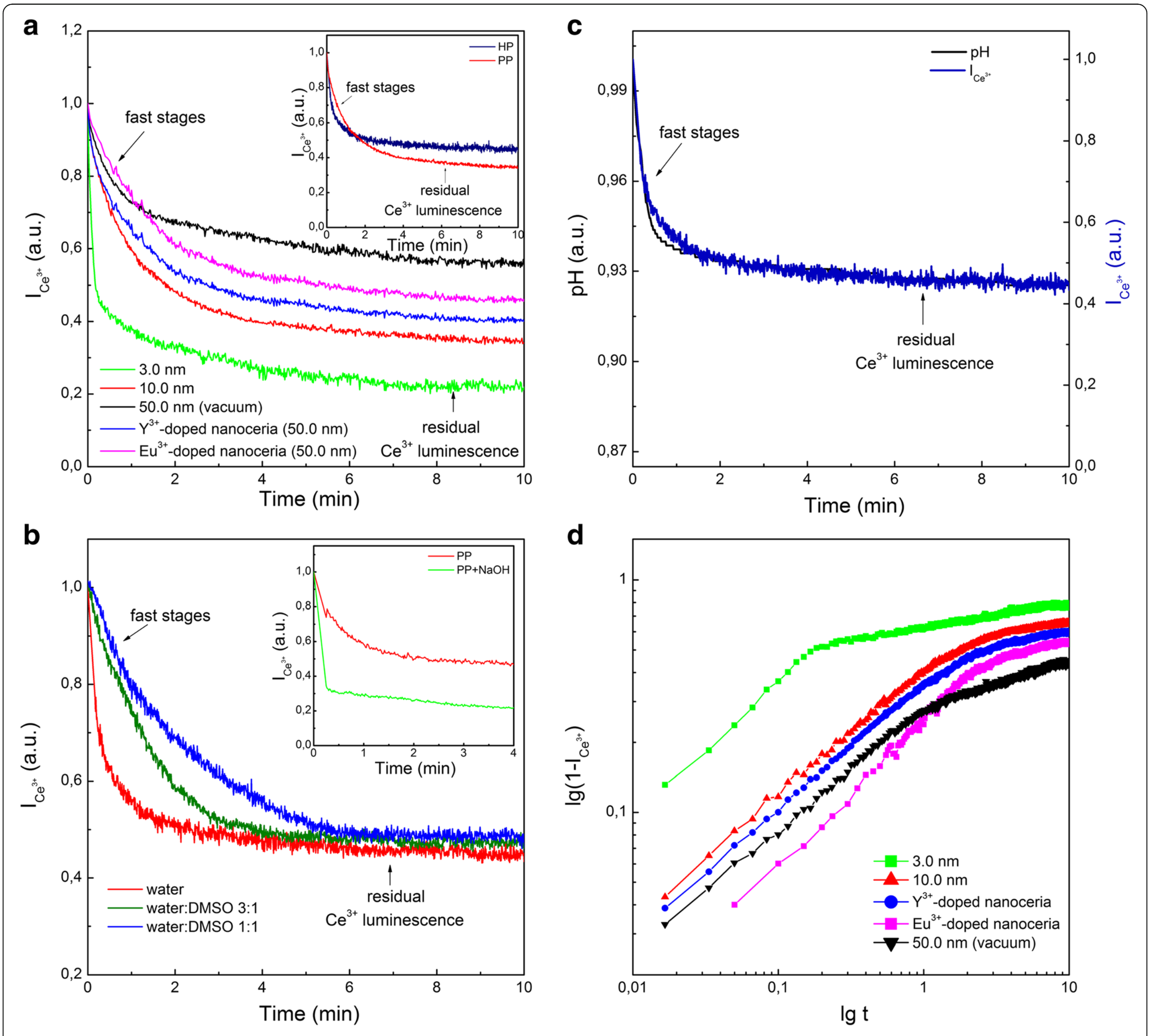

Fig. 2 Time evolution of Ce^{3+} luminescence under the oxidant action (C = 0.1 mM) for different specimens of nanoceria. **a** After HP addition; insert—after HP and PP addition; **b** after PP addition to 10.0-nm nanoceria in water-DMSO solutions; insert—after PP addition and after NaOH and subsequent PP addition. **c** pH and Ce^{3+} band intensity ($I_{Ce^{3+}}$) after PP addition for 10.0-nm nanoceria. **d** Curves of nanoceria filling by oxygen $\rho(t)=1-I_{Ce^{3+}}(t)$ shown on a log-log plot using data shown in **a**

source of H^+ in the case of HP application, we have also revealed the exact coincidence of the pH decrease with the Ce^{3+} band intensity drop under the nanoceria oxidation by PP (Fig. 2c). These facts indicate the water splitting, which can proceed with high efficiency with participation of the $Ce^{4+}-V_O^{++}-Ce^{4+}$ (or $Ce^{4+}-V_O^{+}-Ce^{3+}$) active sites on the nanoceria surface forming as a result of the oxidation of Ce^{3+}-V_O-Ce^{3+} sites (Fig. 3) [13]. There are two possible ways for that (Fig. 3): either the O^{2-} ion occupies V_O^{++} and two H^+ ions are ejected to the solution or the O^{2-} ion occupies V_O^{+} resulting in the creation of hydroxyl, which makes one H^+ ion to be ejected to solution (Fig. 3). The first jump of oxygen into nanoceria regenerates the $Ce^{3+}-V_O-Ce^{3+}$ site for a new oxidation cycle (Fig. 3). This process can be repeated many times with different rates depending on oxidant concentration. The curve $\rho(t) = 1-I_{Ce^{3+}}(t)$ describes the filling of nanoceria with oxygen, and its initial stage fits well the $\sim t^{1/2}$ function (see Fig. 2d). It means that oxygen penetrates into the nanoceria by the single-file diffusion through V_O channels (Fig. 3), where oxygen atoms cannot bypass each other [22, 23]. The formation of large V_O clusters opened onto the oxygen-terminated planes of nanoceria (Fig. 3) is unavoidable for two reasons: all tested nanoceria specimens contain high enough V_O concentrations close to the percolation threshold [24] and V_O concentration reaches its maximum value near the nanoceria surface [10–12]. The linear structures [25, 26] observed for the subsurface V_O may be considered as V_O channels or as components of large V_O clusters.

The pronounced oscillations of the Ce^{3+} band intensity are observed when the oxidant (HP or PP) concentration in colloidal solutions exceeds ~ 0.5 mM, so that the dynamics of nanoceria $Ce^{3+} \rightarrow Ce^{4+}$ oxidation transform to $Ce^{3+} \leftrightarrow Ce^{4+}$ redox scenario (Fig. 4). These oscillations did not appear immediately after the HP ($C = 1.0$ mM) or PP ($C = 1.0$ mM) addition but started to develop when the fast stage comes to completion (Fig. 4a, b). For all oxidants, after the oscillations disappeared, they could be repeated by adding new portions of the oxidant to the colloidal solutions (Fig. 4c). For comparison, the oscillations of the Ce^{3+} band intensity for all tested nanoceria specimens are shown in Fig. 4d. The base lines in Fig. 4d are actually the levels of the residual Ce^{3+} luminescence for each nanoceria specimen (Fig. 2a), and the Ce^{3+} band intensity oscillates above these levels. The variation of V_O concentration in the Y^{3+} (or Eu^{3+})-doped 50.0-nm nanoceria showed clearly that the oscillations of the Ce^{3+} band intensity were observable only when the V_O concentrations became equivalent to those in the 10.0-nm nanoceria (Fig. 4d). In the case of Eu^{3+}-doped 50.0-nm nanoceria the oscillations were more irregular and less pronounced (Fig. 4d). As it was mentioned earlier, this fact is consistent with the suppression of oxygen diffusion in the presence of Eu^{3+} ions [14, 15]. In the annealed 50.0-nm nanoceria with thermodynamically nonequilibrium V_O, the oscillations were not observed at all. The oscillations (see Fig. 4) were observable at the temperatures above 35 °C only.

The observed oscillations (Fig. 4) appeared when the population of V_O by oxygen accumulated during the fast stage (Figs. 2a and 4a) became strongly nonequilibrium. The growth of the first peak of oscillations (Fig. 4a, b) is accompanied by the release of excess oxygen, and as long as the oscillations are observed, the nanoceria releases (Ce^{3+} luminescence increase) and uptakes (Ce^{3+} luminescence decrease) oxygen. For the

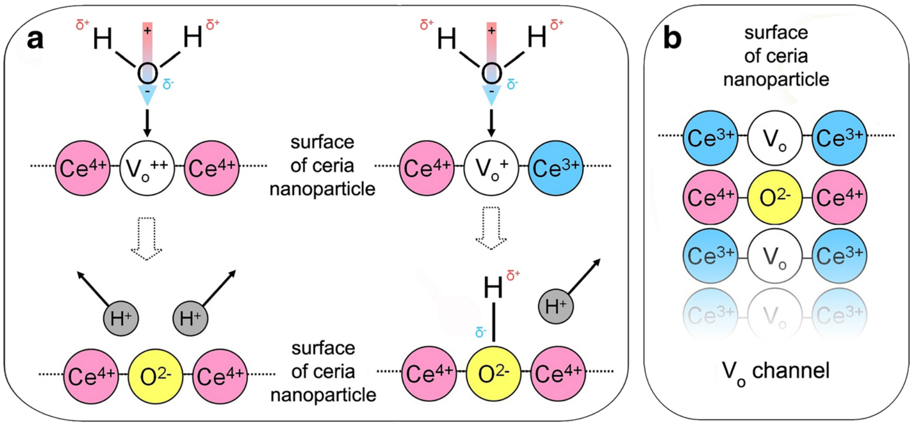

Fig. 3 The stages of the nanoceria interaction with oxidant and water molecule. **a** Double-oxidized $Ce^{4+}-V_O^{++}-Ce^{4+}$ site and single-oxidized $Ce^{4+}-V_O^{+}-Ce^{3+}$ site on nanoceria surface and their interaction with H_2O molecule. **b** Regeneration of $Ce^{3+}-V_O-Ce^{3+}$ site for next oxidation cycle

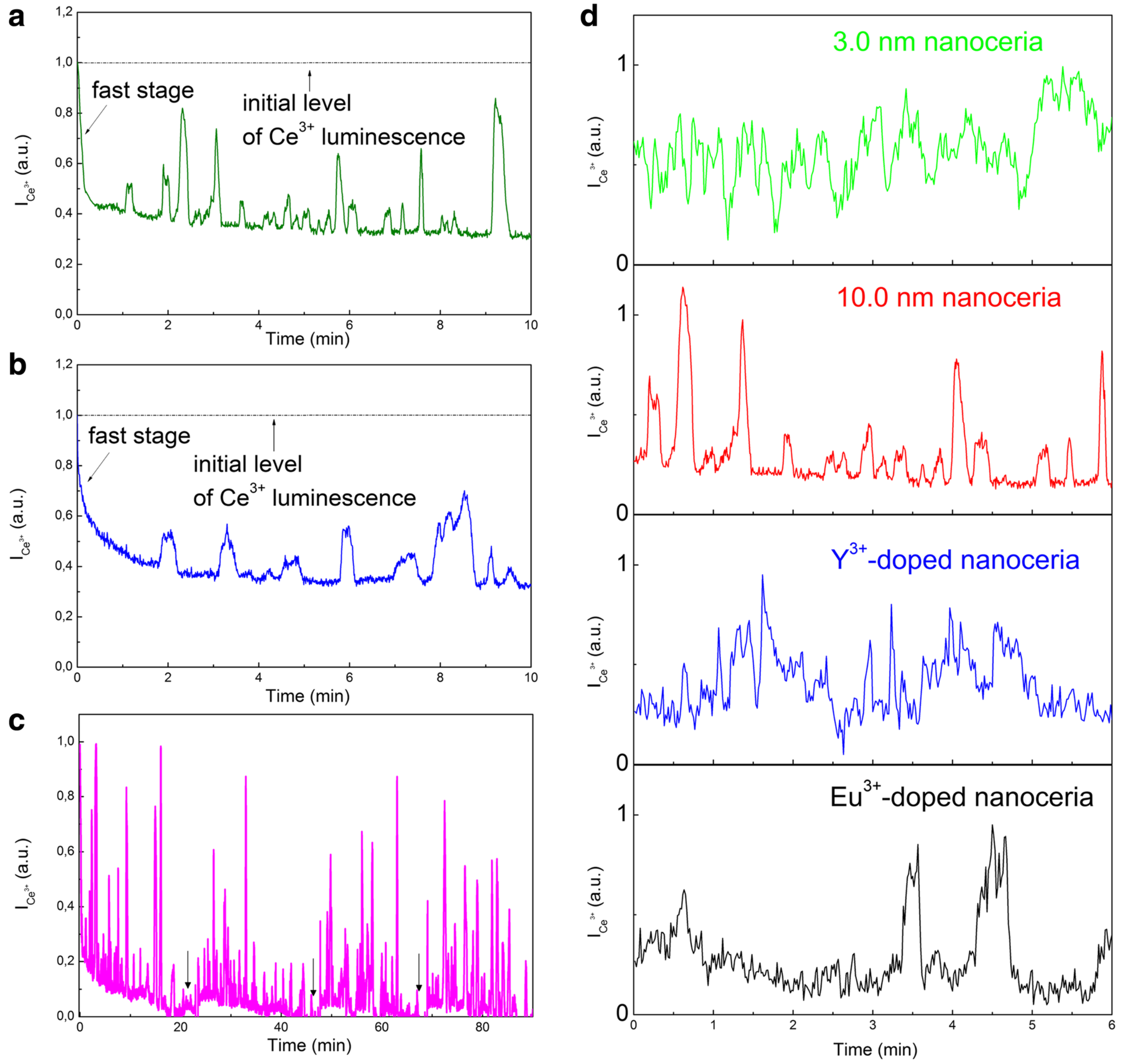

Fig. 4 The oscillations of Ce^{3+} band intensity ($I_{Ce^{3+}}$) stimulated by oxidant (C = 1.0 mM) in colloidal nanoceria: **a** after HP addition for 10.0-nm nanoceria; **b** after PP addition for 10.0-nm nanoceria; **c** after multiple HP addition for 10.0-nm nanoceria; **d** after HP addition for different nanoceria samples

annealed 50.0-nm nanoceria, the phase of oxygen release and, hence, the $Ce^{4+} \leftrightarrow Ce^{3+}$ oscillations are impossible because the thermodynamically nonequilibrium V_O are irreversibly healed by oxygen accumulated during oxidation (Figs. 2a and 4).

It should be noted that the time scale of the Ce^{3+} band intensity evolution (see Figs. 2 and 4) requires an anomalously high rate of oxygen diffusion in nanoceria at RT. Generally, in oxides, the ordinary oxygen diffusion is too slow owing to the large value of the activation energy [14, 15]. But in our case, the fast oxygen diffusion is provided by the loading-dependent reduction of the activation energy inherent for single-file diffusion [23]. The oxidant concentration in the colloidal solutions controls this effect via the rate and level of the filling of V_O clusters with oxygen.

Conclusions

Our results suggest new vision of microscopic mechanisms behind the nanoceria redox performance. First of all, both the surface Ce^{3+} ions available for the oxidant and the deep-seated Ce^{3+} ions are involved in the oxidation dynamics of nanoceria due to oxygen diffusion supported by the open V_O clusters. Such V_O

clusters are inevitably formed at a sufficiently small size (< 15 nm) of nanoceria that explains the strong size dependence of nanoceria antioxidant activity. The self-regeneration (reverse $Ce^{4+} \rightarrow Ce^{3+}$ reduction) of nanoceria in biological environment is a result of releasing the oxygen accumulated during its oxidation by ROS. Similar to the oscillations in heterogeneous catalysis [27], the oscillations of cerium oxidation state in nanoceria can be exploited for the development of high-performance antioxidants, which are extremely important for cell protection under high-intensity radiation (cancer radio-treatment, nuclear catastrophes, etc.). Overall, the ideas suggested in the paper allow to initiate a rational search for new nanomaterials that can be utilized not only as effective antioxidants, but also as unique catalytic materials in various technological areas.

Methods

Methods of Nanoceria Synthesis

Colloidal Synthesis of 3.0- and 10.0-nm Nanoceria

Aqueous solutions of ceria nanoparticles were obtained by the following method: $CeCl_3$ solution (100 ml, 2 mM) was mixed with 100 ml of hexamethylenetetramine solution (4 mM) and stirred by means of magnetic stirrer for 3 h at room temperature. After that, 1.8 ml NH_4OH and 0.6 ml of H_2O_2 were added into the solution. Then, the solution was put in round-bottom flask and refluxed for 5 h. As a result, transparent colorless solutions were obtained. The solution was evaporated in a rotary evaporator flask under vacuum at the bath temperature of 70 °C to 30 ml. A solution of 2 M NaCl was added to the obtained solution until the resulting solution became turbid. Then, the solid phase was precipitated by centrifugation. The precipitate was separated, and solution of sodium chloride was added again. The procedure of precipitate cleaning was repeated three times. After the last stage of centrifugation, solution of sodium citrate with molar ratio CeO_2/NaCt of 1:1 was added to the precipitate. Size of nanoceria obtained from the mixture of cerium (III) chloride and hexamethylenetetramine (HMTA) taken in mole ratio 1:10 was ~ 10.0 nm. At further increase of HMTA, excess size of obtained nanoparticles decreases to ~ 3.0 nm. CeO_{2-x} nanoparticles were stabilized by sodium citrate with molar ratio 1:1. The solutions were additionally dialyzed for 24 h against deionized water to remove the excess of ions and organics species. Dialysis membrane tubing with a molecular weight cutoff of “Cellu Sep H1” 3.5 KDa was used. All sols were transparent in transmitted light and passed through membrane filters with pores of 100 nm without loss.

Sol–gel Synthesis of 50.0-nm Nanoceria

CeO_{2-x}, CeO_2:Eu^{3+}/Y^{3+}(0.1–10 at.%) nanocrystals were obtained by Pechini method. Cerium oxide (CeO_2) (99.995%, Sigma-Aldrich) was dissolved in the mixture of nitric acid (HNO_3) and hydrogen peroxide (H_2O_2) (in 1:1 volume ratio) at 60 °C. Europium oxide (Eu_2O_3) (99.999%, Sigma-Aldrich) and yttrium oxide (Y_2O_3) (99.999%, Sigma-Aldrich) were dissolved in the dilute HNO_3 at 80 °C. The solution of 0.75 g of citric acid and 1 ml of ethylene glycol was added to 20 ml of cerium nitrate $Ce(NO_3)_3$ ($C = 1$ M) solution or to 20 ml the stoichiometric mixture of cerium nitrate $Ce(NO_3)_3$ ($C = 1$ M) and europium nitrate $Eu(NO_3)_3$/yttrium nitrate $Y(NO_3)_3$ ($C = 1$ M) solutions. All the resulting mixtures were treated at 80 °C during 10 h and then hydrolyzed by means of 10 mass.% NH_3 aqueous solution. The precipitates were dried at 120 °C during 5 h and then dehydrated at 250 °C during 4 h. The nanocrystals were annealed during 2 h in vacuum at 1000 °C. After annealing, nanoparticles were dispersed in water at 1 g/l concentration.

Experimental Techniques

The photoluminescence of all types of nanoceria has been excited by a continuous-wave GKL-4UM He-Cd laser ($\lambda \sim 325$ nm) and registered using the SDL-1 grating monochromator with the Hamamatsu R9110 PMT in the photon-counting mode.

Immediately after oxidant (hydrogen peroxide or potassium periodate) addition to aqueous colloidal solutions of nanoceria, the time evolution of Ce^{3+} luminescence intensity (taken at 390 nm) was determined by means of time-resolved measurements at CW excitation (He–Cd laser). Concentrations of nanoceria in aqueous solutions were similar in all experiments and equal to 1 g/l. Concentration of oxidant required to initiate non-reversible $Ce^{3+} \rightarrow Ce^{4+}$ redox reaction was equal to 0.1 mM; concentrations of oxidants for initiation of reversible $Ce^{3+} \leftrightarrow Ce^{4+}$ redox reactions were equal to 1.0 mM for both H_2O_2 (HP) and KIO_4 (PP).

The time dependence of pH value for the nanoceria aqueous colloidal solutions after oxidant addition was measured using pH meter. As the oxidants HP ($C = 0.1$ mM) and PP ($C = 0.1$ mM) were used, pH values were recorded with time intervals of 1 s after addition of the portions of oxidant to nanoceria aqueous colloidal solutions. The time dependence of pH value for distilled water after addition of the oxidant was taken as a control (initial pH value of distilled water was the same as the one for colloidal solutions of nanoceria (pH = 7)).

All experiments were realized at $T = 37$ °C.

Additional file

Additional file 1. Supplementary materials. (DOCX 1515 kb)

Abbreviations

HP: Hydrogen peroxide; PP: Potassium periodate; ROS: Reactive oxygen species; V_O: Oxygen vacancies

Authors' Contributions

The idea of the mechanism of oscillations and antioxidant activity of nanoceria was developed by YM in assistance with NS. Nanocrystals were synthesized by VK. Spectroscopic investigations and interpretation of spectral bands were done by PM and VS. Manuscript was written by YM in assistance with VS. All authors read and approved the final manuscript.

Competing Interests

The authors declare that they have no competing interests.

Publisher's Note

Author details

[1]Institute for Scintillation Materials, National Academy of Sciences of Ukraine, 60 Nauky Ave, Kharkiv 61001, Ukraine. [2]Zabolotny Institute of Microbiology and Virology, National Academy of Sciences of Ukraine, 154 Akademika Zabolotnogo St, Kyiv 03680, Ukraine.

Received: 25 July 2017 Accepted: 8 October 2017

References

1. Gai S, Li C, Yang P, Lin J (2013) Recent progress in rare earth micro/nanocrystals: soft chemical synthesis, luminescent properties, and biomedical applications. Chem Rev 114:2343–2389
2. Tong X, Zhou Y, Jin L, Basu K, Adhikari R, Selopal GS, Zhao H, Sun S, Vomiero A, Wang ZM, Rosei F (2017) Heavy metal-free, near-infrared colloidal quantum dots for efficient photoelectrochemical hydrogen generation. Nano Energy 31:441–449
3. Reed K, Cormack A, Kulkarni A, Mayton M, Sayle D, Klaessig F, Stadler B (2014) Exploring the properties and applications of nanoceria: is there still plenty of room at the bottom? Environ Sci: Nano 1:390–405
4. Fu Q, Saltsburg H, Flutzani-Stephanopoulos M (2003) Active nonmetallic Au and Pt species on ceria-based water-gas shift catalysts. Science 301:935–938
5. Rzigalinski BA, Meehan K, Davis RM, Xu Y, Miles WC, Cohen CA (2006) Radical nanomedicine. Nanomedicine 1:399–412
6. Celardo I, Pedersen JZ, Traversa EL, Ghibelli L (2011) Pharmacological potential of cerium oxide nanoparticles. Nano 3:1411–1420
7. Das S, Dowding JM, Klump KE, McGinnis JF, Self W, Seal S (2013) Cerium oxide nanoparticles: applications and prospects in nanomedicine. Nanomedicine 8:1483–1508
8. Pulido-Reyes G, Rodea-Palomares I, Das S, Sakthivel TS, Leganes F, Rosal R, Seal S, Fernández-Piñas F (2015) Untangling the biological effects of cerium oxide nanoparticles: the role of surface valence states. Sci Rep 5(15613):1–14
9. Nelson BC, Johnson ME, Walker ML, Riley KR, Sims CM (2016) Antioxidant cerium oxide nanoparticles in biology and medicine. Antioxidants 5(15):1–21
10. Tsunekawa S, Ishikawa K, Li ZQ, Kawazoe Y, Kasuya A (2000) Origin of anomalous lattice expansion in oxide nanoparticles. PhysRevLett 85:3440–3443
11. Wu L, Wiesmann HJ, Moodenbaugh AR, Klie RF, Zhu Y, Welch DO, Suenaga M (2004) Oxidation state and lattice expansion of CeO_{2-x} nanoparticles as a function of particle size. Phys Rev B 69(125415):1–9
12. Deshpande S, Patil S, Kuchibhatla S, Seal S (2005) Size dependency variation in lattice parameter and valency states in nanocrystalline cerium oxide. Appl Phys Lett 87:1–3
13. Esch F, Fabris S, Zhou LT, Montini T, Africh C, Fornasiero P, Comelli G, Rosei R (2005) Electron localization determines defect formation on ceria substrates. Science 309:752–755
14. Trovarelli A (2013) Fornasiero P catalysis by ceria and related materials. Imperial College Press, London
15. Nakayama M, Martin M (2009) First-principles study on defect chemistry and migration of oxide ions in ceria doped with rare-earth cations. PhysChemChemPhys 11:3241–3249
16. Coduri M, Scavini M, Allieta M, Brunelli M, Ferrero C (2013) Defect structure of Y-doped ceria on different length scales. Chem Mater 25:4278–4289
17. Chavan SV, Mathews MD, Tyagi AK (2004) Phase relations and thermal expansion studies in the ceria–yttria system. J Am Ceram Soc 87:1977–1980
18. Sharma A, Varshney M, Park J, Ha TK, Chae KH, Shin HJ (2015) Bifunctional $Ce_{1-x}Eu_xO_2$ ($0 \leq x \leq 0.3$) nanoparticles for photoluminescence and photocatalyst applications: an X-ray absorption spectroscopy study. Phys Chem Chem Phys 17:30065–30075
19. Seminko V, Masalov A, Maksimchuk P, Klochkov V, Bespalova I, Viagin O, Malyukin Y (2016) Spectroscopic properties of nanoceria allowing visualization of its antioxidant action. Nanomaterials for Security 149–157
20. Masalov A, Viagin O, Maksimchuk P, Seminko V, Bespalova I, Aslanov A, Malyukin Y, Zorenko Y (2014) Formation of luminescent centers in CeO_2 nanocrystals. J Lumin 145:61–64
21. Lakowicz JR (2006) Principles of fluorescence spectroscopy. Springer, New York
22. Lacasta AM, Sancho JM, Sagues F, Oshanin G (2000) Propagation dynamics of a particle phase in a single-file pore. MRS Proc 651:T9–T1
23. Borman VD, Teplyakov VV, Tronin VN, Tronin IV, Troyan VI (2000) Molecular transport in subnanometer channels. JETP 90:950–963
24. Stauffer D (1994) Aharony a introduction to percolation theory. Taylor and Francis, London
25. Murgida GE, Ganduglia-Pirovano MV (2013) Evidence for subsurface ordering of oxygen vacancies on the reduced CeO_2 (111) surface using density-functional and statistical calculations. PhysRevLett 110(246101):1–5
26. Namai Y, Fukui KI, Iwasawa Y (2003) Atom-resolved noncontact atomic force microscopic observations of CeO_2 (111) surfaces with different oxidation states: surface structure and behavior of surface. J Phys Chem B 107:11666–11673
27. Schüth F, Henry BE, Schmidt LD (1993) Oscillatory reactions in heterogeneous catalysis. Adv Catal 39:51–127